Novel scaffolds for Dual specificity tyrosine-phosphorylation-regulated kinase (DYRK1A) inhibitors

Journal:	*Journal of Medicinal Chemistry*
Manuscript ID	jm-2017-01847p.R3
Manuscript Type:	Article
Date Submitted by the Author:	n/a
Complete List of Authors:	Czarna, Anna; Faculty of Health Sciences, The Arctic University of Norway, Department of Pharmacy Wang, Jinhua; Dana-Farber Cancer Institute, Department of Cancer Biology Zelencova, Diana; University of Tromsø, The Norwegian Structural Biology Centre, Department of Chemistry Liu, Yao; Dana-Farber Cancer Institute, Department of Cancer Biology Deng, Xianming; Dana-Farber Cancer Institute, Department of Cancer Biology Choi, Hwan Geun; Dana-Farber Cancer Institute, Department of Cancer Biology Zhang, Ting-hu; Dana-Farber Cancer Institute, Department of Cancer Biology Zhou, Wenjun ; Dana-Farber Cancer Institute, Department of Cancer Biology Chang, Jae Won; Dana-Farber Cancer Institute, Department of Cancer Biology Kildalsen, Hanne; Faculty of Health Sciences, The Arctic University of Norway, Department of Pharmacy seternes, Ole-morten; Universitetet i Tromso Helsevitenskapelige fakultet Helsefak, Pharmacy Gray, Nathanael; Dana Farber Cancer Institute, Cancer Biology; Harvard Medical School, Dana-Farber Cancer Institute Engh, Richard; University of Tromsoe, Chemistry Rothweiler, Ulli; University of Tromsø, The Norwegian Structural Biology Centre, Department of Chemistry

Novel scaffolds for Dual specificity tyrosine-phosphorylation-regulated kinase (DYRK1A) inhibitors

Anna Czarna[1], Jinhua Wang[2], Diana Zelencova[3,†], Yao Liu[2], Xianming Deng[2], Hwan Geun Choi[2], Tinghu Zhang[2], Wenjun Zhou[2], Jae Won Chang[2], Hanne Kildalsen[1], Ole Morten Seternes[1], Nathanael S. Gray[2], Richard A. Engh[3] and Ulli Rothweiler[3]*

[1]Department of Pharmacy, Faculty of Health Sciences, The Arctic University of Norway, N-9037 Tromsø, Norway

[2]Department of Cancer Biology, Dana-Farber Cancer Institute, Department of Biological Chemistry and Molecular Pharmacology, Harvard Medical School, Boston, MA 02115, USA

[3]The Norwegian Structural Biology Centre, Department of Chemistry, UiT, The Arctic University of Norway, N-9037 Tromsø, Norway

[†]Current address: Department of Physical Organic Chemistry, Latvian Institute of Organic Synthesis, Aizkraukles 21, LV-1006, Riga, Latvia

ABSTRACT

DYRK1A is one of five members of the Dual-specificity tyrosine (Y) phosphorylation-Regulated Kinase (DYRK) family. The DYRK1A gene is located in the Down syndrome critical region and regulates cellular processes related to proliferation and differentiation of neuronal progenitor cells during early development. This has focused research on to its role in neuronal degenerative diseases, including Alzheimer's and Down syndrome; recent studies have also shown a possible role of DYRK1A in diabetes. Here we report a variety of scaffolds not generally known for DYRK1A inhibition, demonstrating their effects in *in vitro* assays and also in cell cultures. These inhibitors effectively block the tau phosphorylation that is a hallmark of Alzheimer's Disease. The crystal structures of these inhibitors support the design of optimized and novel therapeutics.

INTRODUCTION

Alzheimer's disease (AD) is the primary cause of dementia in the elderly[1]. AD affects less than 5% of individuals 65 years of age and younger, but the incidence of AD reaches nearly 40% in patients 85 years of age and older[1]. This neurodegenerative disorder is characterized by neuronal death and loss of gray matter in the frontal cortex and hippocampus. This neurodegenerative disorder is characterized by neuronal death and loss of gray matter in the frontal cortex and hippocampus. Memory loss is a typical symptom of AD and has been linked to the accumulation of amyloid plaques and neurofibrillary tangles (NFTs)[2]. The latter process is mediated by hyperphosphorylation of tau proteins that are inactive and form multiple aggregates. According to the β–amyloid cascade hypothesis, the deposition of insoluble β-amyloid is responsible for neuronal death. Plaques are constituted by β-amyloid peptides (Aβ) that are generated via the cleavage of the amyloid precursor protein (APP) by β- and γ-secretases. Aβ-fragments, 37-42

amino acids in length, may produce soluble oligomers, although they aggregate into insoluble β-amyloid plaques in AD[2, 3]. Alternatively, the insoluble hyperphosphorylated tau proteins and the buildup of NFTs may be the etiology of neuronal death[4-6]. Both mechanisms of neuronal pathology depend on the kinase DYRK1A, which regulates the cell cycle, neuronal differentiation and synaptic transmission[7].

Increased levels of DYRK1A are present in the brain of patients with AD and in other neurodegenerative diseases, including Parkinson, Huntington and Pick syndromes[7]. The human *DYRK1A* gene is located in the Down syndrome critical region (DSCR) encoded by chromosome 21, and the overexpression of DYRK1A likely contributes to the neurological abnormalities of this disorder[8].

DYRK1A increases the secretase-mediated cleavage of APP into Aβ peptides. DYRK1A phosphorylates APP directly[9] and the Aβ peptides stimulate DYRK1A expression in a positive feedback loop[9]. Additionally DYRK1A phosphorylates presenilin 1 (PSEN1)[10], one of the four core proteins in the γ-secretase complex, which enhances secretase activity. DYRK1A phosphorylates human microtubule associated protein tau at eleven different sites[11], whereby most of the tau protein becomes hyperphosphorylated. The initial phosphorylation of tau by DYRK1A triggers tau phosphorylation by GSK3β, which potentiates self-aggregation and fibril formation *in vitro*[11, 12]. Because of the central role of DYRK1A in the development and progression of AD, DYRK1A has emerged as a high priority target for inhibition, offering a novel approach for the treatment of AD. In recent years, evidence has built up that point to a role of DYRK1A in diabetes and β-cell proliferation[13-15], expanding the pharmaceutical application of a DYRK1A inhibitor. Therefore, we screened a diverse set of scaffolds for their ability to inhibit DYRK1A kinase activity and to prevent tau phosphorylation. The diversity of the novel scaffolds

and the binding modes determined by crystal structure and *in vitro* assays may lead to the development of novel strategies for the clinical treatment of AD.

RESULTS

Identification of novel DYRK1A inhibitors

Novel DYRK1A inhibitors were identified by employing KinomeScan™ screening data of an in-house library of approximately 1,000 compounds including previously synthesized kinase inhibitors. 23 compounds were chosen as candidates for activity assay and their ability to inhibit the phosphorylation of DYRKtide (RRRFRPASPLRGPPK) by DYRK1A at a fixed concentration of 20 μM with an ATP regenerative assay (Cook et al.[16]). The results for the most promising compounds are shown in **Table 1** and all the 23 compounds are shown in the supporting information **Table S1**. The inhibitors had a broad range of activity: 8 compounds showed strong inhibition (remaining activity <5%), 8 compounds showed moderate inhibition (11%-46% remaining activity) and 6 compounds showed little or no inhibition (70%-100% remaining activity). 15 inhibitors that showed at least 50% inhibition were titrated in decreasing concentrations (200μM-20nM) to determine the IC_{50} and K_i values.

Compounds **AC12**, **AC13**, **AC14**, **AC15** and **AC27** were found to possess highest ability to inhibit the phosphorylation of DYRKtide, with K_i values around 100-250 nM. **AC7**, **AC24** and **AC25** inhibitors showed K_i values of around 326 nM - 570 nM. Inhibitors with identical core scaffolds revealed similar K_i values, as seen for the two pairs **AC12** and **AC15** (~104 nM and ~158 nM), and **AC24** and **AC25** (383 nM and 575 nM, respectively). The remaining compounds (**AC2**, **AC8**, **AC16**, **AC18**, **AC20**, **AC22**, and **AC23**) were weaker compared to the 8 inhibitors

discussed above and exhibited K_i values ranging from 1.7 µM to >8 µM (supporting information **Table S1**).

Table 1. Inhibitory activity of the selected most active compounds.

Code	Name	Remaining activity at 20 µM (%)	IC_{50} (nM)	K_i (nM)	Kinome Scan 10 µM	Kinome Scan 1 µM	Cell line tau phosphorylation	Cell line Luciferase Assay***	PDB code
AC22	XMD8-49	24	>6000	>2800	0.7	-	active	5-10 µM	6EIL
AC23	XMD8-62e	15	4200	2015	1.6	-	active	0.5-1 µM	6EIP
AC20	HG-8-60-1	11	3500	1680	1.2	-	active	>20 µM	6EIJ
AC25	XMD15-27	4	1200	575	0.15	-	active	†	6EIR
AC24	XMD14-124	1.3	800	383	0.05	-	active	10-20 µM	6EIQ
AC27	JWC-055	2	532	252	-	1.4	active	0.05-0.1 µM	6EIS
AC15	XMD7-112	0	329	158	**	-	active	5-10 µM	6EJ4
AC12	XMD7-117	0	216	104	**	-	active	1-5 µM	6EIF
AC28	JWD-065*	-	-	-	0	-	-	-	6EIV

IC_{50} values determined in the Cook assay at 25 degrees and 128 µM ATP, Ki calculated with a K_M value for DYRK1A of 118 µM[17]. *due to solubility problems of the compound in stock solution and resulting uncertainty of the concentration, binding kinetics were not measured, however a cocrystal structure with inhibitor could be obtained. **values available for DYRK1B only (0.5 and 0.2 respectively). *** Concentration where inhibitory activity was above 1.5 fold the basal level. †compound failed to inhibit DYRK1A in this assay, negatively interferes with the cells.

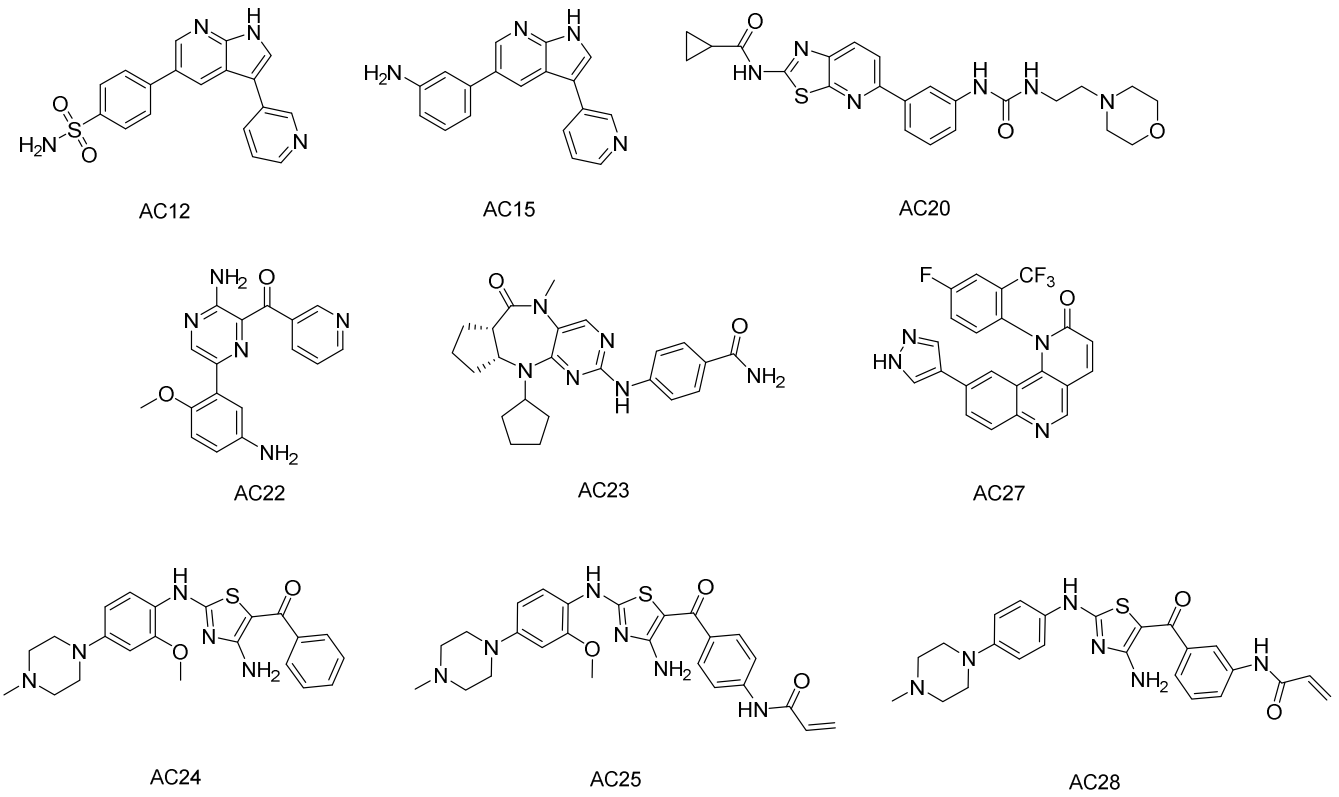

Figure 1. Structures of the nine novel DYRK1A inhibitors, representing six different core scaffolds. **AC12** and **AC15** share one core structure, and **AC24**, **AC25** and **AC28** share a second type of the core structure.

Tau phosphorylation inhibitory activity assay in cells

Eight compounds that displayed inhibitory activity *in vitro* (**see Table 1**) were further tested in a cell line to establish whether they possessed the capacity to inhibit tau phosphorylation by DYRK1A. Expression vectors encoding FLAG-tagged TAU and EGFP-tagged DYRK1A were co-transfected into NCI-H1299 cells and the amount of phospho-tau protein (p-tau) was analyzed by Western blot (**Figure 2** and supporting information **Figure S2).** Cells transfected with empty vectors were utilized as controls.

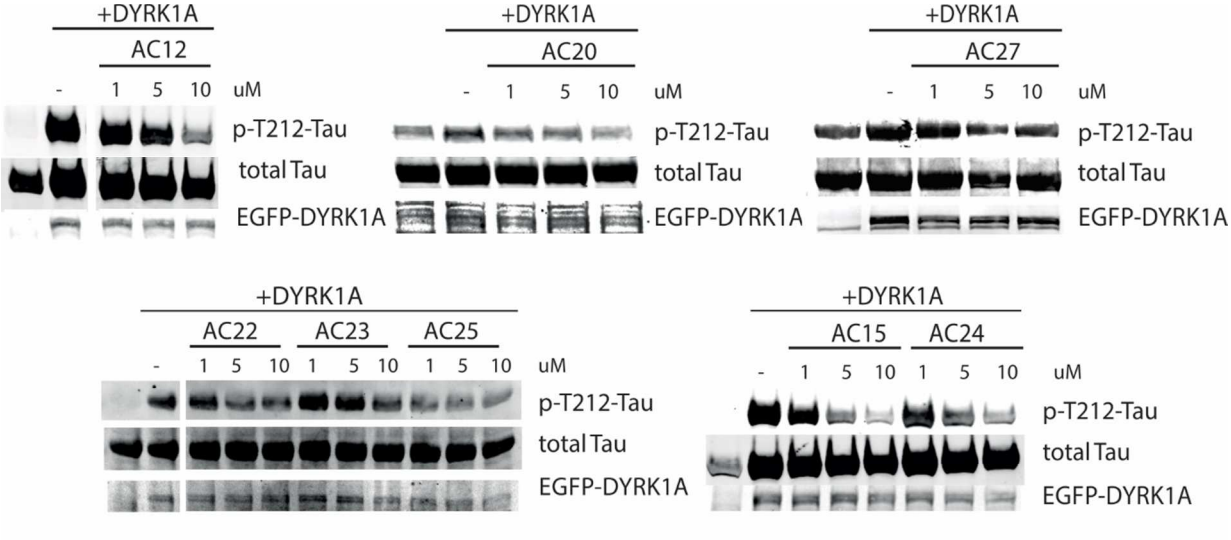

Figure 2. Inhibition of DYRK1A dependent tau T212 phosphorylation by different compounds. NCI-H1299 cells were transfected with expression vector encoding FLAG-tagged tau in combination with either empty expression vector or EGFP-tagged DYRK1A. Twenty hours after transfection the cells were incubated for 2 hours with vehicle (-) or the indicated inhibitor concentration before the cells were harvested. Phosphorylated T212 tau was detected by Western-blotting using the polyclonal anti-phospho T212 tau antibody (44-740G, Invitrogen), total FLAG-tau was detected by using a monoclonal M2 anti-FLAG antibody (F1804, Sigma-Aldrich) and EGFP-DYRK1A by a polyclonal anti-GFP antibody (Sc-8334, Santa-Cruz).

AC12, **AC15**, **AC24** and **AC25** showed a significant dose-dependent inhibition of pT212-tau phosphorylation, in contrast to **AC20**, **AC22**, **AC23** and **AC27**. However, all these compounds inhibited pT212-tau phosphorylation. The degree of kinase inhibition observed at the protein level reflected the one seen in the *in vitro* activity assay. In general, compounds with K_i of 600 nM or tighter showed clear dose-response effects, while compounds with K_i values ranging from 1.7 to 3 μM showed inhibition but with significantly greater noise with respect to dose-response correlation. An exception to this general observation is **AC27**. This compound inhibits DYRK1A in the pT212-tau phosphorylation assay, however not as potently as it would have been expected from the *in vitro* activity assay.

Crystal structures

The inhibitors were set up in co-crystallization trials with DYRK1A. Nine of the novel scaffolds (**Figure 1**) formed co-crystals. The crystal packing and asymmetric unit is similar to the previously published DYRK1A complexes with PKC412[17] or the benzothiazole fragments[18], with tetramers constituting the asymmetric unit. In general, the best electron density fit is found for protomer A and the greatest disorder is seen in protomer C. Several chains in the asymmetric unit show disulfide bridge formation between the HCD motif and the activation loop cysteine. However, in many chains the cysteine residues are reduced and/or in a mixed state, with additional evidence of radiation damage due to low amplitude electron density for cysteine C312[17, 18]. The compounds are bound to all four protomers in the tetramer of the asymmetric unit in DYRK1A (**Figure 3**). One exception is compound **AC22**, which lacks electron density for the entire inhibitor in chain C of the tetramer and the ATP-pocket is empty. However, the electron

density is clear for the other three chains. The omit difference density maps after simulated annealing for all the nine inhibitors are shown in the supporting information **Figure S3**. The crystallographic data and refinement statistics are summarized in supporting information **Table S2** in the supplementary data.

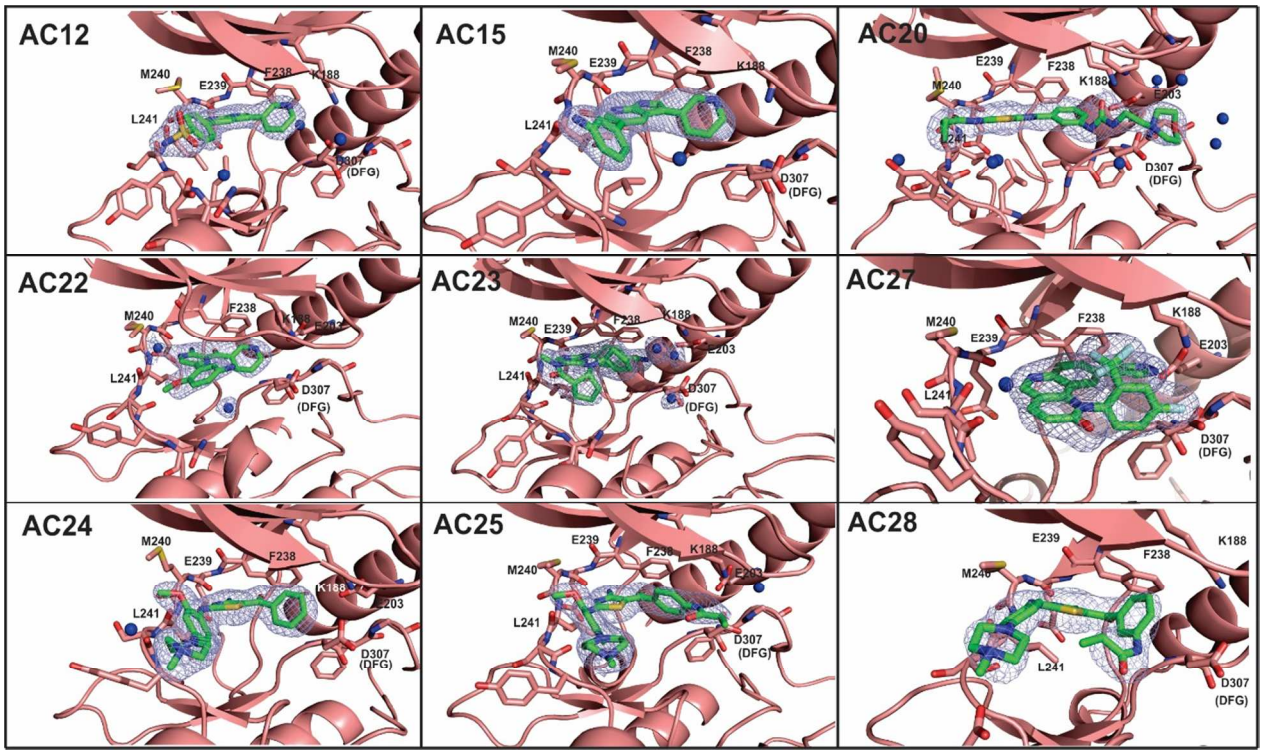

Figure 3. Binding pocket of DYRK1A bound to nine different inhibitors. The electron density for the inhibitor (2Fo-Fc map) is shown at 1 σ. The inhibitors form hydrogen bonds to E239 and L241, and **AC20**, **AC22** and **AC27** form an H-bond to K188. Inhibitors **AC12** and **AC15** have a hydrogen bond acceptor group oriented toward K188. Most of inhibitors are shown as they bind to chain A of the four protein molecules in the asymmetric unit of DYRK1A. The two exceptions are **AC23** where the inhibitor is shown bound in chain B, and **AC27** with the inhibitor shown in chain D. In the **AC23** crystal structure, only chain B has a water clearly visible in the electron density that could form bridging H-bonds between the inhibitor and K188 or D307. In the **AC27**

crystal structure chain D has a water molecule, which connects the inhibitor to the hinge. There is no clear electron density for a water in the other chains, however, some diffuse electron density might suggest water molecules at these positions, in the other chains too. PDB codes for DYRK1A complexes: **AC12**: 6EIF; **AC15**: 6EJ4; **AC20**: 6EIJ; **AC22**: 6EIL; **AC23**: 6EIP; **AC24**: 6EIQ; **AC25**: 6EIR; **AC27**: 6EIS; **AC28**: 6EIV.

The inhibitors that could be co-crystallized with DYRK1A represent six different chemical scaffolds. Inhibitors **AC12** and **AC15** share a 3-(3-pyridin-3-yl-1H-pyrrolo[2,3-b]pyridin-5-yl)phenyl core scaffold, while inhibitors **AC24**, **AC25** and **AC28** share a 4-[4-amino-2-[2-methoxy-4-(4-methylpiperazin-1-yl)anilino]-1,3-thiazole-5-carbonyl]phenyl core scaffold. **AC12** and **AC15** differ by the substitutions of sulfonamide (para) or amine (meta) on the terminal arene, respectively. Compound **AC24** represents the core scaffold, whereby compounds **AC25** and **AC28** have terminal acrylamide functions added to the terminal arene at para and meta positions, respectively. **AC28** differs additionally by the lack of a methoxy substitution on the central phenyl ring. The other core scaffolds are represented by compounds **AC20** with 7-azathiazole, **AC22** as a pyrazine, **AC23** with an alkaloid, and **AC27** as a substituted 1,6-phenanthroline.

With one exception, the inhibitors are typical hinge binders (**Figure 3 and supporting information Figures S3, S4 and S5**). **AC12** and **AC15** each make two hydrogen bonds to E239 (gatekeeper+1) and L241 (gatekeeper+3). The pyridine nitrogen faces the catalytic lysine K188, but the 4 Å distance to the amine nitrogen is too long for a hydrogen bond. **AC22** is anchored to the hinge via two hydrogen bonds, which orients the pyridine nitrogen H-bond acceptor towards the catalytic lysine K188. Compared to **AC12** and **AC15**, the distances to K188 are shorter, including one contact at 3.2 Å, within the range of typical hydrogen bond distances. The crystal

structure also shows that K188 shares a salt bridge with E203. Similarly, the aminopyrimidine functionality of **AC23** is anchored to the hinge, which points the benzamide substituent towards K188, but without a direct hydrogen bond interaction. However, in chain B there is a water molecule that bridges the gap between the amide and K188. The benzamide moiety has a parallel displaced π-π stacking interaction with the gatekeeper phenylalanine F238.

AC24, **AC25** and **AC28** make three hydrogen bonds to the hinge via the thiazole and two adjoining amines. In addition, the piperazine rings of these compounds have salt bridge interactions with D247 (the gatekeeper+8 residue). They do not interact with K188. Compared to **AC24**, the addition of an acrylamide group on **AC25** weakens binding, and the crystal structure shows no favorable interactions, and especially no covalent binding. A superposition of **AC24**, **AC25**, and **AC28** from all asymmetric unit domains show that the acrylamide groups are pushed out of the binding pocket (**Figure 4**). However, the electron density for the acrylamide groups are relatively weak, and some divergence in their positions is evident in the refined structures. A rotation of the terminal benzene ring of approximately 90 degrees may be seen in two binding poses for **AC25**. The other benzene ring of the scaffold (adjacent to the piperazine ring) is oriented differently and heterogeneously for **AC28**. The methoxy substituent of this ring, found in **AC24** and **AC25**, apparently stabilizes this benzene ring compared to **AC28** (**Figure 4**). On the other hand, the ring of inhibitor **AC28** is stabilized by intramolecular π-π interactions of the acrylamide double bond with the π system of the benzene ring.

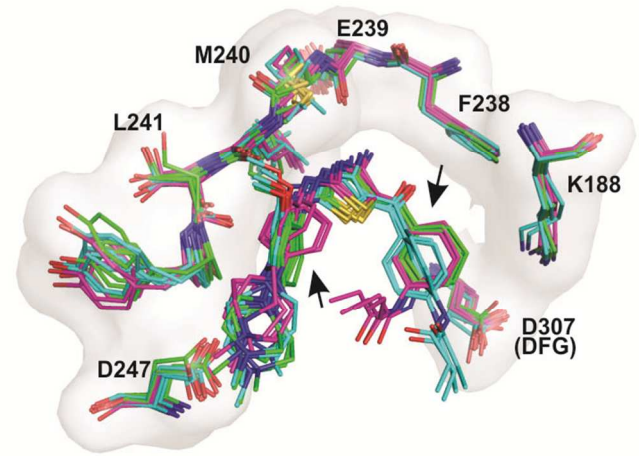

Figure 4. Superposition of the binding pockets and inhibitors of the four chains in the asymmetric unit of DYRK1A of each inhibitor: **AC24** (green PDB: 6EIQ) with **AC25** (cyan PDB: 6EIR) and **AC28** (violet PDB: 6EIV). Although the general pose of each inhibitor remains similar, some differences are evident between the individual pockets. **AC24** has the greatest conservation of geometry, while especially the acrylamide groups of **AC25** and **AC28** show more variation, reflected also by lower electron density for these parts.

AC20 has only a single hinge binding hydrogen bond, with L241 (gatekeeper+3), rather than a pair (including the gatekeeper+1 residue E239) that is typical for the other inhibitors. **AC20** shares a hydrogen bond with the catalytic lysine K188 with its urea oxygen, and also shares a salt bridge with the DFG aspartate D307 via the morpholine nitrogen. It forms in addition a perpendicular π stacking interaction with the gatekeeper phenylalanine. Like all the other inhibitors, **AC20** binds in a typical type I binding mode.

The strongest of the inhibitors in this study, **AC27** uniquely has no hydrogen bond to the hinge. It has anchoring hydrogen bonds with K188 and E203 via its diazole group, with N244 via its carbonyl group, and also with the N292 side chain as a C-H--O hydrogen bond with a hydrogen

of the fluorinated arene. Additionally, a bridging water between the hinge and the inhibitor was found in the chain D of the tetramer. This water has a hydrogen bonding distance of 2.7 Å from the 1,6-phenanthroline nitrogen, and is in contact with the main chain amide nitrogen of L241 with a distance of 2.8 Å and to the carbonyl of E239 of 2.6 Å. The trifluoromethyl, fluorobenzyl ring is in perpendicular face-edge intramolecular contact with both the 1,6-phenanthroline and diazole rings. The trifluoromethyl group is embedded in a shallow hydrophobic pocket created by the first glycine (G166) of the glycine rich loop, the preceding I165 side chain, and the V173 side chain opposite of G166. (**Figure 3**) A superposition of all the inhibitors is shown in supporting information **Figure S4.**

Kinase profiling of DYRK1A inhibitors

We evaluated kinase selectivity profiles as determined by KinomeScan™ binding assays against a panel of 353/402/442 distinct kinases and their mutants (**Figure 5**). The kinase profiling data for the inhibitors show that **AC12** and **AC15** are pan kinase inhibitors (with a broad spectrum of inhibition). As a consequence, these two inhibitors did not show a clear pattern of selectivity, and were generally less effective against tyrosine kinases. The kinase profiling data for remaining seven of the compounds with cocrystal structures showed the typical cross reactivities of the inhibitors between DYRK and CLK families. In addition, **AC22** and **AC27** show significant cross reactivities against GSK3β, which is consistent with the kinase selectivity pattern of leucettine L41[19]

AC20 exhibited good overall kinome selectivity, with a S(10) selectivity score of 0.06 at 10 μM. (The S(10) selectivity index is defined as the percentage of the kinome inhibited below 10% of the control; S[10] = [number of kinases with %Ctrl < 10]/[number of kinases tested]). **AC20**

binds CLK2 more tightly than DYRK1A. This compound bound also the tyrosine kinases ABL and PDGFR, which is unsurprising, considering that the series of compounds with this core structure were initially designed for targeting BCR-ABL[20].

AC22 is the only tested inhibitor that shows a stronger inhibition of GSK3β compared to DYRK1A. Other kinases of the CMGC group significantly inhibited by **AC22** include CLK2, HIPK1/2 and CDK7. **AC22** also interferes with other kinases across several families, albeit with weaker binding affinity.

AC23 exhibited rather weak and unspecific DYRK binding. The main targets of this compound belonged to the CMGC and CAMK families, with DRAK1/2 and ERK5 as the top hits.

The three thiazole compounds, **AC24**, **AC25** and **AC28**, have slightly varying affinities. While **AC24** had greater affinity for DYRKs compared to CLKs, the addition of the acrylamide in **AC25** and **AC28** shifted the profile towards CLK2, and also decreases the overall selectivity.

AC27, an analog of mTOR inhibitor Torin2[21], selectively binds to mTOR, but also CMGC family kinases and lipid kinases PIK3CG, PIK4CB, with S(10) scores of 0.03 at 1 μM. It possesses similar inhibition strengths against DYRK1A/B, CLK1/3 and GSK3A/B among CMGC family members.

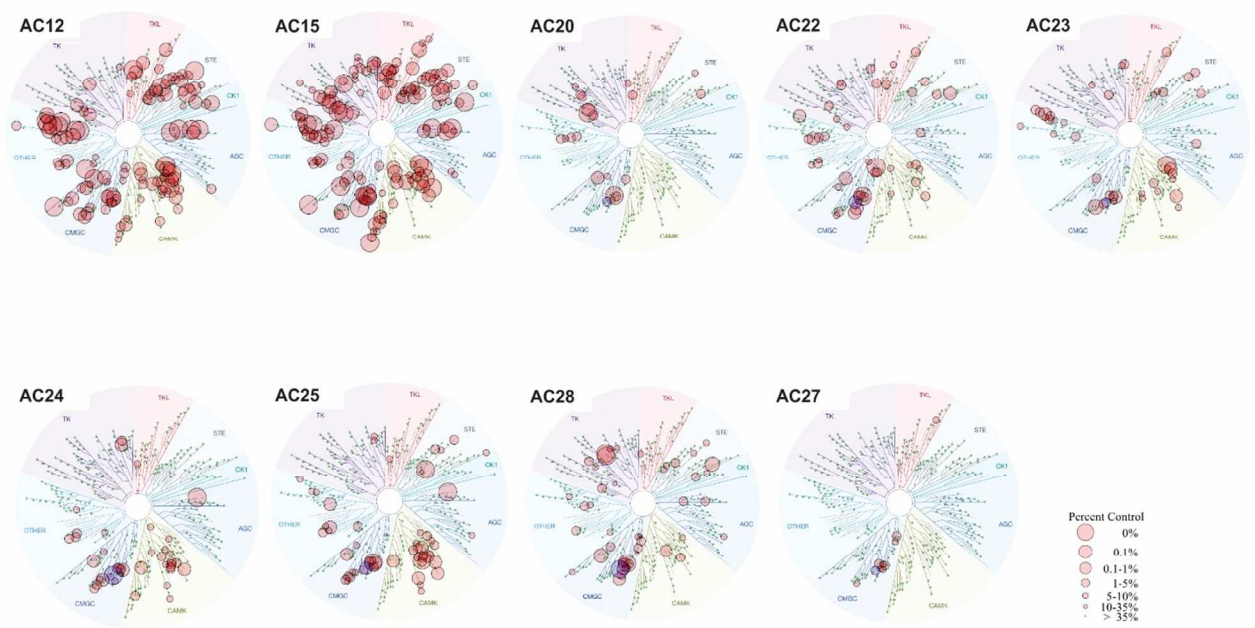

Figure 5 Kinome binding plots for the nine compounds. The levels of binding were measured at concentrations 10 μM (except for **AC27**, measured at 1 μM).

NFAT Luc reporter assays

The newly identified compounds were studied in the HEK293 cell line by introducing the NFAT luciferase activity assay (**Figure 6**). The compounds were titrated in increasing amounts from 0.25 μM to 20 μM. **AC27**, as the most active compound, was titrated from 0.05 μM to 10 μM. With the exception of **AC25**, all compounds showed activity in the tested cell line. **AC12** was found to be active at concentrations up to 5 μM; higher concentrations of this compound led to a drop in the activity, suggesting that **AC12** might be toxic at concentrations >5 μM. **AC15**, despite sharing the same core structure of **AC12**, showed dose-dependent inhibition up to 20 μM; this compound required a minimum of 5 μM to show considerable activity above the background level. This was also the case for **AC20**, **AC22** and **AC24**. Based on the NFAT luciferase activity assay, the most active compounds were **AC23** and **AC27**. Specifically, **AC27** showed clear activity at 50 nM and thus is approximately 10-fold more active than **AC23** and approximately

100-fold more active than to the other six inhibitors in this assay. The drop in the activity of **AC27** at 10 µM and **AC23** at 20 µM may suggest that these concentrations might be toxic. As mentioned above, **AC25** was the only inactive compound with respect to this assay, showing an apparent dose-dependent drop in the basal activity, possibly coupled with toxicity for HEK293 cells.

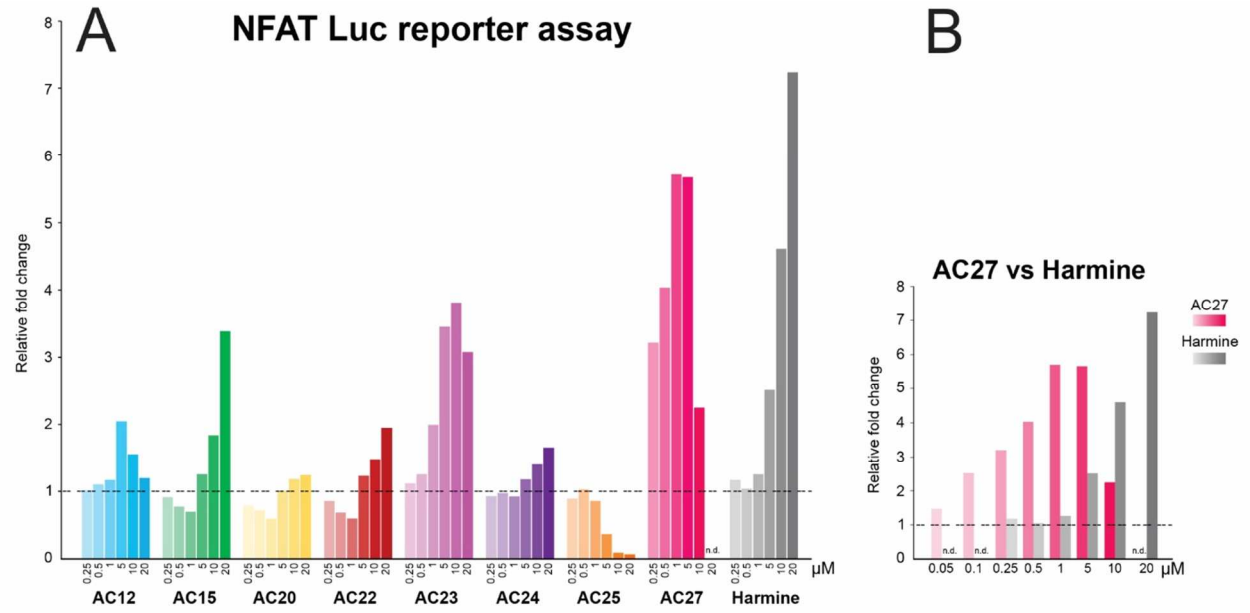

Figure 6. NFAT Luc reporter assay. The plot is normalized to the basal activity of the luciferase. Numbers indicate the fold of increase in luciferase activity upon inhibition of DYRK1A (**A**). The most active compound **AC27** shows a 1.5fold increase in luciferase activity at 50 nM. For comparison harmine is included in the same assay (**B**). Even though harmine reached a higher activity and does not display the drop in activity as **AC27** at higher concentrations toward DYRK1A, **AC27** is active at much lower concentrations. 100 nM **AC27** leads to the same activity as 5 µM harmine, making **AC27** nearly 50 times more active than harmine in this particular cellular assay.

DISCUSSION

The list of potential DYRK1A inhibitors has been growing over the past few years. Diverse chemical fragments that bind to DYRK1A with high affinity have been reported[22]. However, none of these have advanced into clinical trials. This study presents a set of novel scaffolds with good potential for DYRK1A inhibition, evaluated using a series of structural and cellular assay experiments. **AC12**, **AC15** and **AC22** are compounds with relatively low molecular weights and can considered as fragments and classical hinge binders. In contrast to harmine, INDY[23] or recently published hydroxy- and methoxy-benzothiazole[18] fragments, the distances of inhibitor atoms to the catalytic lysine or the aspartate from the DFG motive remain relatively long. On the other hand, structural variations in the physiological environment might include significant dynamic hydrogen bonding to the catalytic lysine K188, especially correlated with dynamic properties of helix C. Although **AC12**, **AC15** and **AC22** have similar molecular weights and similar binding poses with the hinge region, their binding strengths differ greatly. **AC12** and **AC15** were the strongest binders, while **AC22** was one of the weakest that still enabled cocrystal structure determination. (The relatively weak binding of **AC22** is also reflected in the fact that one of the ATP pockets of the four DYRK1A chains in the asymmetric unit of the crystal structure was empty). Detailed comparison of the structures **AC12**, **AC15** and **AC22** shows that the pyridine rings occupy the same volume, and the overlap of the nitrogen atoms anchored to the hinge is apparent (**Figure 7A**). However, the methoxy group of **AC22** on the aniline ring most likely weakens the binding. The structure shows that the methoxy group pushes the compound away from the hinge, hence increasing intramolecular strain.

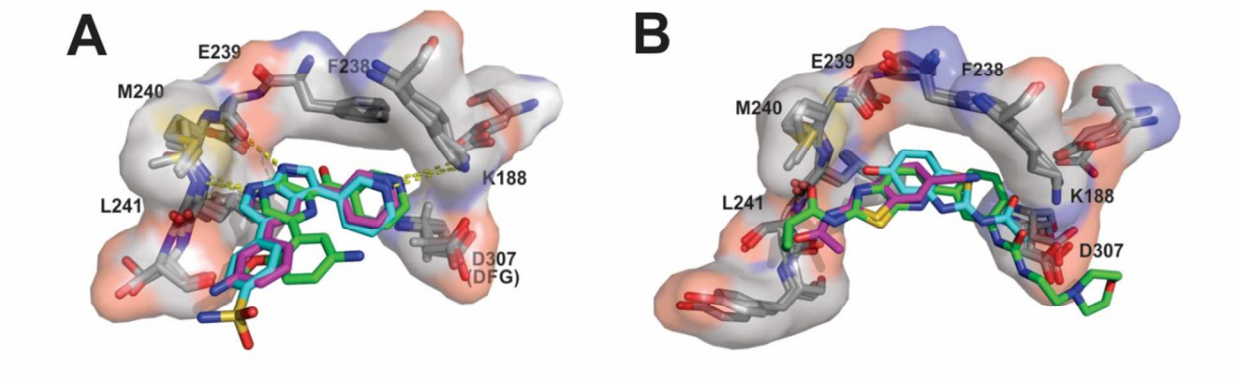

Figure 7. Orientation and interaction of the inhibitors in the binding pocket. (A) Superimposition of **AC12** (cyan PDB: 6EIF) **AC15** (pink PDB: 6EJ4) and **AC22** (green PDB: 6EIL). The methoxy group of **AC22** displaces the inhibitor away from the hinge, weakening binding. (B) Superposition of **AC20** (green PDB: 6EIJ) with 5-hydroxy-benzothiazole (blue PDB: 5A3X) and 6-cyano-benzothiazole (magenta PDB: 5A4T). **AC20** binds with its 5-substiuted pyridothiazole in the same orientation as the 6-cyano-benzothiazole and, unlike 5-hydroxy-benzothiazole or INDY, does not make sulfur aromatic ring interactions with the gatekeeper phenylalanine. The three compounds also have differing selectivity profiles. While **AC12** and **AC15** are more nearly pan kinome inhibitors (targeting many different kinases), **AC22** is much more discriminating, with however a greatly reduced inhibitory strength.

The remaining inhibitors for which a cocrystal structure could be obtained are selective towards the CMGC kinase group and DYRKs. However, all show additional cross reactivity against targets outside the CMGC group.

Inhibitor **AC20** inhibits DYRK1A, however the strongest inhibition of CMGC group kinases is of CLK2, and similar or stronger inhibition is seen of TK group members ABL and PDGFRB (with considerable variation across ABL mutants). **AC20** is clearly hydrogen bonded to K188,

wrapping its extended tail across and partially around the DFG motif. The pyridothiazole core structure of **AC20** is similar to the benzothiazoles found in other published DYRK1A inhibitors (including INDY[23], BINDY[24], or the recently published 5- or 6- substituted benzothiazole fragments[18]), but differs by an additional nitrogen in the six membered ring. **AC20** is a 6-substituted pyridothiazole; analogous to the benzothiazole interactions , the pyridothiazole binds alongside the hinge instead of making sulfur aromatic ring interactions with the gatekeeper as seen for INDY[23] or the 5-substituted fragments of benzothiazoles[18] **(Figure 7B**).

The three thiazole compounds **AC24**, **AC25** and **AC28** show intermediate binding strengths and selectivity. Compound **AC24** represents the core scaffold in this group, whereby compounds **AC25** and **AC28** have terminal acrylamide functions added to the terminal arene at para and meta positions, respectively. The addition of the acrylamide in **AC25** and **AC28** shifted the binding affinity away from DYRK towards CLK2, and also decreases the overall selectivity. Acrylamides as functional groups are typically used to introduce covalent binding of inhibitors via addition to cysteines. (These compounds were previously synthesized as inhibitors of kinases other than DYRK1A) Because of the absence of cysteine at the ATP pocket in DYRK1A, the acrylamides in **AC25** and **AC28** are not expected to introduce covalent binding, but nonbonded interactions still affect binding strengths. The functional acrylamide group might stabilize binding to related off-targets. **AC25** was the only compound that did not inhibit DYRK1A in the NFATluc assay, instead showing toxicity.

As described above, the crystal structure of **AC25** showed that the additional acrylamide was associated with a shift of its parent phenyl ring away from its position in **AC24**, presumably to avoid a steric clash with D307 (of DFG), but possibly colliding with V173. Two characteristics distinguish **AC28** from **AC24** and **AC25**: the acrylamide functional group at the meta position, and the lack of a 2-methoxy substituent in aniline. These properties changed the inhibition

selectivity pattern significantly, eliminating their inhibitory activity against many CAMK family kinases, JNK kinases, and adding the binding to the pseudokinase domains of JAK1 and TYK2. Moreover, the cross reactivity towards MAST1 in the AGC group of **AC24** and **AC25** was lost in **AC28**. These clear and specific dependencies warrant further more detailed structural studies.

AC23 and **AC27** have a potential bridging water molecule in the binding pocket that could be an important affinity determinant. In fact, for **AC27** the water in the binding pocket is the only apparent interaction that anchors **AC27** to the hinge. The waters are unambiguous only in chain B (**AC23**) or chain D (**AC27**) in the electron density of the DYRK1A tetramer. Despite the missing electron density, a water bridging interaction may however be important, because multiple bridged geometries may exist. Optimization of these compounds can take this into account (**Figure 3 and 8**).

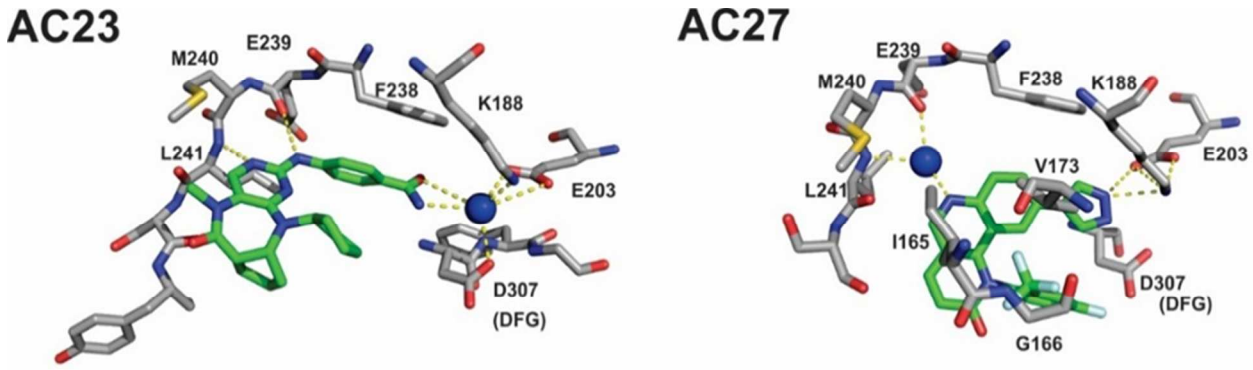

Figure 8 Water mediated binding of **AC23** (PDB: 6EIP) and **AC27** (PDB: 6EIS) to DYRK1A. The structure of the inhibitor in the ATP pocket of DYRK1A includes a water molecule that enables bridging interactions between the inhibitor and the K188, E203 and D307 for **AC23**, and between the inhibitor and the hinge carbonyl of E239 and amide nitrogen of L241 for **AC27**. There is no clear electron density for a water in the other chains; however, some diffuse electron density suggests it to be present there also.

AC23 and especially **AC27** were the most active compounds in the cell line assay (NFATluc, Figure 6). These compounds were active at lower concentrations compared to harmine. **AC23** reached a twofold activity increase at 1 μM, and **AC27** reached twofold activation already at 0.1 μM. In contrast, harmine reaches this level only at ~5 μM, i.e. **AC23** and **AC27** may be seen as 5x and 50x as active, respectively. On the other hand, both **AC23** and **AC27** show reduced activity at concentrations above 10 μM. This could be an indication that these higher concentrations introduce toxicity to the cells, while harmine continues to exhibit dose dependent inhibition at these concentrations.

As mentioned above, several DYRK1A inhibitors were identified in the recent past, but none of these compounds has met the selectivity standards needed for use as probe molecules. Harmine, one of the most commonly used inhibitors in DYRK1A related research, has strong cross inhibition of monoamine oxidase that would create severe side effects. The low selectivity also makes harmine unsuitable as a probe to test DYRK1A inhibition in cell lines. Efforts to eliminate the MAO inhibition while keeping the DYRK1A inhibition lead to the harmine derivative AnnH75[25]. Another DYRK1A inhibitor, green tea flavonol epigallocatechin-gallate (EGCG), was shown to correct cognitive deficits in Down syndrome mouse models and in humans[26]. However, it also potentially has multiple targets (and correspondingly is under consideration for use a broad range of disorders) and cannot be considered a DYRK specific inhibitor. The compounds EHT1610 and EHT5372 are among the most selective DYRK inhibitors identified so far[27, 28]. Crystal structures of these compounds in complex with a kinase are available for DYRK2 (5LXD and 5LXC). A comparison of this scaffold to AC27, one of the more selective compound in our series, shows some remarkable similarities. First, a structural comparison of the EHT1610 and EHT5372 compound bound to DYRK2 suggests that the canonical hinge binding may be less

essential for high affinity binding in DYRK[28] as it is for AC27, because its hinge interaction is only indirect, via a bridging water molecule. Secondly, all three compounds interact with the P-loop, and the trifluoromethyl in AC27 or the 2-fluoro- and 2-chloro-benzyl group of EHT1610 and EHT5372 occupy the same space. One major difference is in the overall orientation of the inhibitors. Considering them "U" or horse-shoe shaped, the opening of the "U" for AC27 points toward the P-loop aryl F160, while the orientation is reversed for the EHT inhibitors. The benzyl rings of AC27 and the EHT inhibitors are roughly perpendicular to each other. (**Figure 9**)

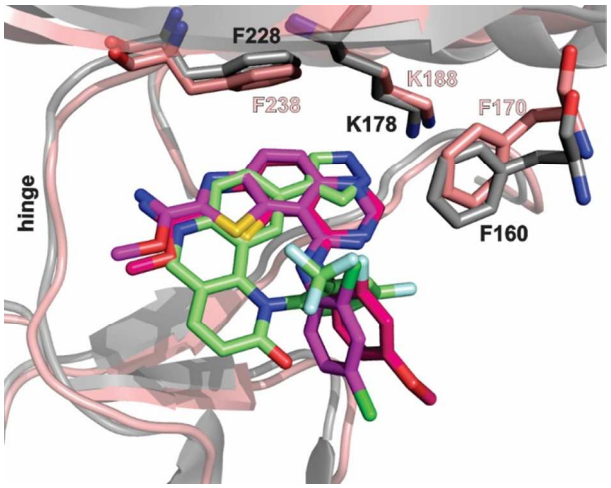

Figure 9 Comparison of the binding of AC27 (light green, PDB: 6EIS) with EHT1610 (red, PDB: 5LXD) and EHT5372 (magenta, PDB: 5LXC); (DYRK1A, salmon; DYRK2, gray).

Additional inhibitors of DYRK1A discussed in the literature include a derivative of a marine sponge alkaloid Leucettine L41, which has shown some efficacy in mice to prevent memory impairment[29]. Benzothiazole fragments[18, 30] and the independently developed benzothiazoles INDY[23] and BINDY[24] are also effective inhibitors of DYRK1A. FINDY is a selective inhibitor of the kinase DYRK1A that targets its folding process[31]. A detailed review article of the most

recent DYRK1A inhibitors summarizes these results[22]. The lead compounds we present here, along with their binding poses as seen in the crystal structures, represent valuable additional resources for DYRK1A inhibitor development and optimization of drug likeness and selectivity profiles.

CONCLUSIONS

Twenty-two new compounds were tested for their ability to inhibit and bind to DYRK1A. These compounds belong to diverse chemical scaffolds of kinase inhibitors and their inhibitory strengths (K_i) vary between 200 nM and >10 μM. Kinase profiling showed that some of the compounds (e.g. **AC12** and **AC15**) have a broad spectrum of kinase inhibition, while others are much more specific against DYRK and CLK2. These new scaffolds offer novel opportunities to design DYRK1A inhibitors. Their inhibitory properties vary across the characterization methods and the results of *in vitro* vs cellular assays, especially the pT212-tau phosphorylation vs. the NFAT Luc reporter assays, were less strongly correlated for the compounds. However, this only underlines the importance to study inhibitors in multiple approaches to find the most effective inhibitor. Newly revealed binding features, such as the CH-O interaction with Asn292, or the bound waters that serve as anchors to the catalytic lysine or the hinge, may provide valuable information for optimization of these inhibitors against DYRK1A and related kinases, targeting Alzheimer's disease and diabetes.

EXPERIMENTAL SECTION

1. Synthesis of the inhibitors

AC15[32], **AC20**[33], **AC23**[34], **AC27**[35] and **AC28**[36] were previously reported as TRK, Bcr-Abl, ERK5, mTOR, and HIPK2 inhibitors, respectively. **AC12**[32] and **AC22**[37] were synthesized following procedure described in references. **AC24** and **AC25** were generated from a common intermediate 1-(4-isothiocyanato-3-methoxyphenyl)-4-methylpiperazine **2**, which was obtained from reaction of 2-methoxy-4-(4-methylpiperazin-1-yl)aniline with triphosgene under basic condition (**Scheme 1**). This isothiocyanate intermediate was allowed to react with cyanamide in the presence of *t*-BuOK, followed by addition of phenacyl bromide to give the desired 2,4-diaminothiazoles **AC24** in one-pot synthesis with 96% yield. Intermediate **3** was synthesized by similar procedure with 4-nitrophenacyl bromide and subjected to primary amine protection to generate **4**. Reduction of nitro group by platinum dioxide gave rise to corresponding aniline analog, which was subjected to acrylation and Boc deprotection to afford **AC25**.

Scheme 1. Synthesis of **AC24** and **AC25**[a]

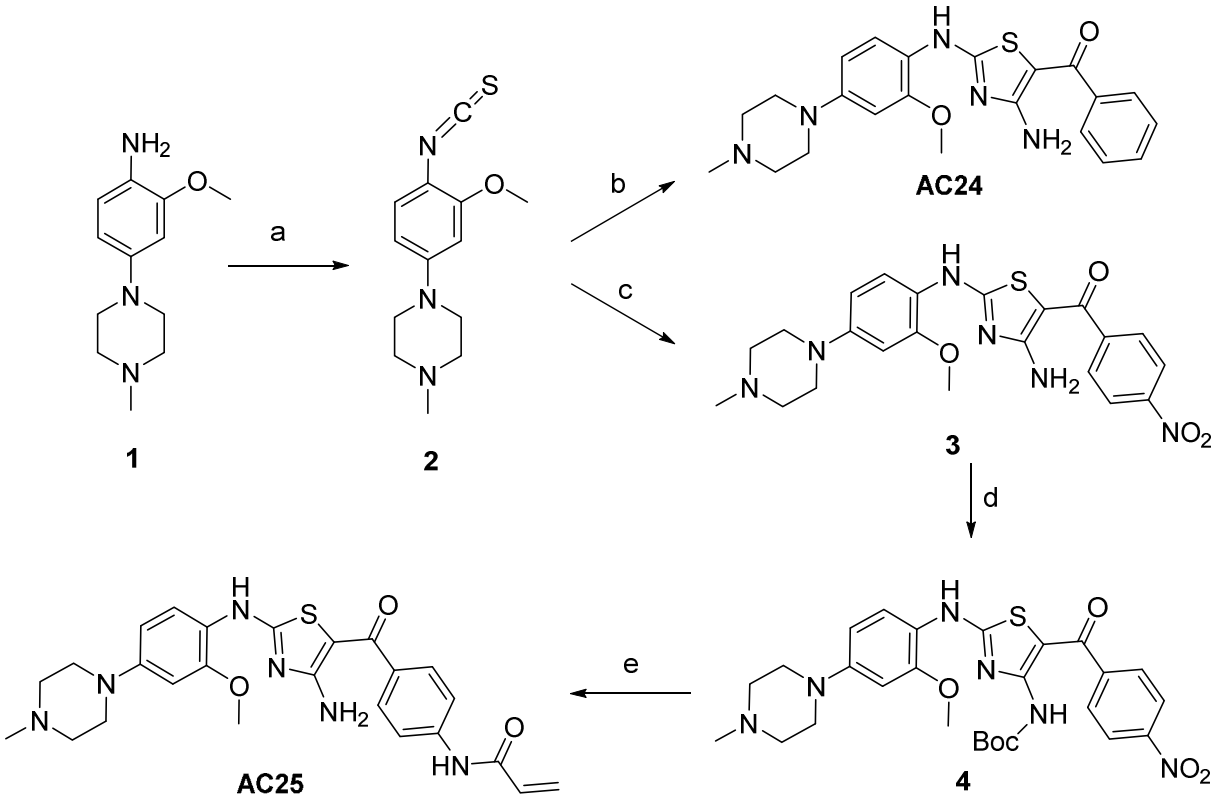

[a]Reaction conditions: (a) 1.0 equiv of thiophosgene, 5.0 equiv of TEA, $CHCl_3$, rt, 3 h, 94%; (b) 1) 2.4 equiv of NH_2CN, 1.5 equiv of *t*-BuOK, acetonitrile, 0 °C to rt, 1 h; 2) 1.0 equiv of 2-bromo-1-phenylethan-1-one, rt, 4 h, 96%; (c) 1) 2.4 equiv of NH_2CN, 1.5 equiv of *t*-BuOK, acetonitrile, 0 °C to rt, 1 h; 2) 1.0 equiv of 2-bromo-1-(4-nitrophenyl)ethan-1-one, rt, 4 h, 47%; (d) 1.0 equiv of $(Boc)_2O$, 0.3 equiv of DMAP, 2.0 equiv of DIEA, CH_2Cl_2, rt, 2 days, 89%; (e) 1) 1.05 equiv of PtO_2, H_2, MeOH, rt, 1 h; 2) 1.27 equiv acryloyl chloride, CH_2Cl_2, 0 °C, 0.5 h; 3) TFA, 0 °C to rt, 1 h, 46%.

2. Chemistry.

Unless otherwise noted, reagents and solvents were obtained from commercial suppliers and were used without further purification. ^{1}H NMR and ^{13}C NMR were recorded on Bruker Ascend 500. ^{1}H NMR spectra were 500 MHz, and chemical shifts are reported in parts per million (ppm,δ) downfield from tetramethylsilane (TMS). Coupling constants (*J*) are reported in Hz. Spin multiplicities are described as s (singlet), d (doublet), t (triplet), m (multiplet), and br (broad). IR spectra were recorded on a Bruker ALPHA II Platinum single reflection diamond ATR Module. High-resolution mass spectra (HRMS) were recorded on a Bruker Impact HD q-TOF Mass Spectrometer. Preparative HPLC was performed on a Waters Symmetry C18 column (19 x 50 mm, 5 μM) using a gradient of 5-95% acetonitrile in water containing 0.05% trifluoroacetic acid (TFA) over 8 min (10 min run time) at a flow rate of 30 mL/min. Analytic HPLC was performed on a SunFire C18 column (4.6 x 150 mm, 3.5 μM) using a gradient of 5-95% acetonitrile in water containing 0.05% trifluoroacetic acid (TFA) over 15 min (17 min run time) at a flow rate of 1.0 mL/min. Purities of compounds were greater than 95% unless indicated otherwise, as determined by analytical HPLC.

4-[3-(Pyridin-3-yl)-1*H*-pyrrolo[2,3-*b*]pyridin-5-yl]benzene-1-sulfonamide (XMD7-117, AC-12). ^{1}H NMR (500 MHz, DMSO-d_6) δ 12.47 (s, 1H), 9.36 (br, 1H), 9.08 – 8.48 (m, 4H), 8.29 (d, J = 2.0 Hz, 1H), 8.05 (d, J = 8.3 Hz, 2H), 7.99 – 7.77 (m, 3H), 7.43 (s, 2H). ^{13}C NMR (126 MHz, DMSO-d_6) δ 149.5, 143.2, 143.2, 142.2, 142.5, 142.4, 138.6, 128.5, 128.1, 127.8, 126.7, 126.6, 117.4, 110.3. IR $\boldsymbol{\nu}_{max}$ (neat): 3299, 3007, 2862, 1586, 1527, 1476, 1329, 1156, 1095, 909, 670, 589, 544 cm^{-1}. HRMS (ESI) *m/z*: calcd for $C_{18}H_{14}N_4O_2S$ $[M + H]^+$, 351.0910; found 351.0909.

5-(5-Amino-2-methoxyphenyl)-3-(pyridine-3-carbonyl)pyrazin-2-amine (XMD8-49, AC-22). ^{1}H NMR (500 MHz, CD_3OD) δ 9.27 (d, J = 1.2 Hz, 1H), 8.84 (s, 1H), 8.70 (d, J = 4.9 Hz, 1H), 8.47 (d, J = 7.9 Hz, 1H), 7.61 (dd, J = 7.9, 5.0 Hz, 1H), 7.10 (d, J = 2.8 Hz, 1H), 6.94 (d, J = 8.7 Hz, 1H), 6.79 (dd, J = 8.6, 2.8 Hz, 1H), 3.83 (s, 3H). ^{13}C NMR (126 MHz, CD_3OD) δ 192.9, 154.7, 150.8, 150.7, 150.3, 149.6, 141.0, 139.9, 138.7, 134.5, 127.6, 125.9, 123.3, 117.1, 116.9, 113.00, 55.3. IR $\boldsymbol{\nu}_{max}$ (neat): 3424, 3252, 3124, 2836, 1632, 1585, 1503, 1222, 1207, 1032, 798, 679, 442 cm^{-1}. HRMS (ESI) *m/z*: calcd for $C_{17}H_{15}N_5O_2$ $[M + H]^+$, 322.1299; found 322.1299.

1-(4-Isothiocyanato-3-methoxyphenyl)-4-methylpiperazine (2) To a solution of 2-methoxy-4-(4-methylpiperazin-1-yl)aniline (**1**) (663 mg, 3.0 mmol) and triethylamine (2.10 mL, 15.0 mmol) in 10 mL $CHCl_3$ at 0 ^{o}C, thiophosgene (0.23 mL, 3.0 mmol) was added. After 15 minutes, the reaction mixture was stirred at room temperature. Once the reaction completed (about 3 hours), the reaction mixture was diluted with ethyl acetate, washed with ice water and brine. After the organic layer was dried with $MgSO_4$, the solvent was removed. The crude product of title compound (747 mg, 94%) was used directly for next step without purification (84.9 % purity). ^{1}H NMR (500 MHz, $CDCl_3$) δ 6.93 (d, J = 8.6 Hz, 1H), 6.38 – 6.26 (m, 2H), 3.81 (s, 3H), 3.20 (t, J = 5.1 Hz, 4H), 2.56 (t, J = 5.0 Hz, 4H), 2.33 (s, 3H). ^{13}C NMR (126 MHz, $CDCl_3$) δ 156.7, 151.3, 137.8, 128.8, 126.1, 107.4, 99.6, 55.9, 54.7, 48.4, 45.9. IR $\boldsymbol{\nu}_{max}$ (neat): 2936, 2794, 2703, 2099, 1595, 1565, 1510, 1417, 1263, 1252, 1211, 1203, 1134, 1025, 1008, 969, 815, 556 cm^{-1}. HRMS (ESI) *m/z*: calcd for $C_{13}H_{17}N_3OS$ $[M + H]^+$, 264.1165; found 264.1165. HPLC: 84.9 % at 254 nM.

(4-Amino-2-((2-methoxy-4-(4-methylpiperazin-1-yl)phenyl)amino)thiazol-5-yl)(phenyl) methanone (XMD14-124, AC24). To a solution of 1-(4-isothiocyanato-3-methoxyphenyl)-4-methylpiperazine (**2**) (30 mg, 0.12 mmol) in 1.0 mL acetonitrile at 0 ^{o}C cyanamide (10 mg, 0.24 mmol) was added, followed by potassium *tert*-butoxide (0.15 mL 1M solution in THF,

0.15 mmol). After 10 minutes, the reaction mixture was stirred at room temperature. Once the reaction completed (about one hour), 2-bromo-1-phenylethan-1-one (20 mg, 0.1 mmol) was added at room temperature. The reaction completed in about four hours. The reaction mixture was diluted with ethyl acetate, washed with ice water and brine. After the organic layer was dried with $MgSO_4$, the solvent was removed and the residue was purified by column purification (CH_2Cl_2/3.5 N Ammonia in MeOH) to afford desired compound (40.7 mg, 96%). ^{1}H NMR (500 MHz, CD_3OD) δ 7.56 – 7.51 (m, 2H), 7.47 (d, J = 8.7 Hz, 1H), 7.40 – 7.24 (m, 3H), 6.56 (d, J = 2.5 Hz, 1H), 6.44 (dd, J = 8.8, 2.5 Hz, 1H), 3.75 (s, 3H), 3.18 (t, J = 5.0 Hz, 4H), 2.74 (t, J = 5.0 Hz, 4H), 2.42 (s, 3H). ^{13}C NMR (126 MHz, CD_3OD) δ 183.8, 172.5, 167.00, 152.8, 150.1, 141.9, 130.1, 128.0, 126.6, 124.4, 120.5, 107.6, 100.4, 94.4, 54.9, 54.2, 48.1, 44.0. IR $\boldsymbol{\nu}_{max}$ (neat): 2806, 1602, 1537, 1213, 1350, 1262, 1241, 737, 699, 509 cm^{-1}. HRMS (ESI) *m/z*: calcd for $C_{22}H_{25}N_5O_2S$ $[M + H]^+$, 424.1802; found 424.1802.

(4-Amino-2-((2-methoxy-4-(4-methylpiperazin-1-yl)phenyl)amino)thiazol-5-yl)(4-nitrophenyl)methanone (3). To a solution of 1-(4-isothiocyanatophenyl)-4-methylpiperazine (**2**) (157.8 mg, 0.6 mmol) in 5.0 mL acetonitrile at 0 ^{o}C cyanamide (50 mg, 1.19 mmol) was added, followed by potassium *tert*-butoxide (0.75 mL 1M solution in THF). After 10 minutes, the reaction mixture was stirred at room temperature. Once the reaction completed (about one hour), 2-bromo-1-(4-nitrophenyl)ethan-1-one (122 mg, 0.5 mmol) was added at room temperature. The reaction completed in about four hours. The reaction mixture was diluted with ethyl acetate, washed with ice water and brine. After the organic layer was dried with $MgSO_4$, the solvent was removed and the residue was purified by column purification (CH_2Cl_2/3.5 N Ammonia in MeOH) to afford desired compound (219 mg, 47%). ^{1}H NMR (500 MHz, $CDCl_3$) δ 8.17 (d, J = 8.3 Hz, 2H), 7.93 (s, 1H), 7.78 (d, J = 8.3 Hz, 2H), 7.39 (d, J = 8.6 Hz, 1H), 6.49 – 6.36 (m, 2H), 3.78 (s,

3H), 3.13 (t, J = 5.0 Hz, 4H), 2.50 (t, J = 5.0 Hz, 4H), 2.28 (s, 3H). ^{13}C NMR (126 MHz, $CDCl_3$) δ 181.5, 170.8, 165.9, 151.2, 150.2, 148.7, 147.3, 128.2, 123.7, 122.1, 119.5, 107.7, 100.0, 55.8, 55.0, 49.1, 46.1. IR $\boldsymbol{\nu}_{max}$ (neat): 2808, 1597, 1533, 1417, 1339, 1262, 1242, 972, 735, 705, 473 cm^{-1}. HRMS (ESI) *m/z*: calcd for $C_{22}H_{24}N_6O_4S$ $[M + H]^+$, 469.1653; found 469.1652.

***tert*-Butyl (2-((2-methoxy-4-(4-methylpiperazin-1-yl)phenyl)amino)-5-(4-nitrobenzoyl) thiazol-4-yl)carbamate (4).** To a stirred suspension of (4-amino-2-((2-methoxy-4-(4-methylpiperazin-1-yl)phenyl)amino) thiazol-5-yl)(4-nitrophenyl)methanone (**3**) (72 mg, 0.15 mmol) in 4.0 mL dichloromethane at room temperature, 4-dimethylaminopyridine (6.0 mg, 0.05 mmol), N,N-diisopropylethylamine (0.06 mL, 0.3 mmol), and di-*tert*-butyl dicarbonate (34 mg, 0.15 mmol) were added. After 10 minutes, the reaction mixture turned clear. When the reaction completed (about 2 days), the reaction mixture was concentrated and the residue was purified by column purification (CH_2Cl_2/3.5 N Ammonia in MeOH) to afford titled compound (93.1% purity, 77 mg, 89%). ^{1}H NMR (500 MHz, CD_3OD) δ 8.39 (d, J = 8.4 Hz, 2H), 7.99 (d, J = 8.4 Hz, 2H), 7.14 (d, J = 8.5 Hz, 1H), 6.77 (d, J = 2.5 Hz, 1H), 6.68 (dd, J = 8.7, 2.5 Hz, 1H), 4.07 – 3.92 (m, 2H), 3.84 (s, 3H), 3.72 – 3.60 (m, 2H), 3.32 – 3.05 (m, 4H), 3.02 (s, 3H), 1.40 (s, 9H). ^{13}C NMR (126 MHz, CD_3OD) δ 184.0, 167.9, 163.9, 155.4, 152.7, 151.5, 149.1, 146.8, 129.7, 128.2, 123.4, 120.5, 107.8, 100.7, 83.9, 54.9, 53.3, 46.5, 42.2, 26.6. IR $\boldsymbol{\nu}_{max}$ (neat): 1717, 1676, 1610, 1520, 1345, 1293, 1127, 1091, 847, 433 cm^{-1}. HRMS (ESI) *m/z*: calcd for $C_{27}H_{32}N_6O_6S$ $[M + H]^+$, 569.2177; found 569.2182.

***N*-(4-(4-Amino-2-((2-methoxy-4-(4-methylpiperazin-1-yl)phenyl)amino)thiazole-5-carbonyl)phenyl)acrylamide (XMD15-27, AC25).** A suspension of *tert*-butyl (2-((2-methoxy-4-(4-methylpiperazin-1-yl)phenyl)amino)-5-(4-nitrobenzoyl)thiazol-4-yl)carbamate (**4**) (50 mg, 0.088 mmol) and platinum dioxide (21 mg, 0.093 mmol) in 6.0 mL methanol was stirred at room temperature under hydrogen atmosphere. After one hour, the reaction mixture was filtered. The

solvent of the filtrate was removed and the residue was dried under vacuum. The crude product was used directly without purification. To its solution in 3.0 mL dichloromethane at 0 ^{o}C acryloyl chloride (9 μL, 0.11 mmol) was added. Once the reaction completed (in about 30 minutes), 1.0 mL trifluoroacetic acid was added at 0 ^{o}C. The temperature of reaction mixture gradually increased to room temperature. When the reaction completed, reaction mixture was concentrated and the resulting residue was purified by reverse-phase prep-HPLC using a water (0.05%TFA)/methanol (0.05% TFA) gradient to afford the desired compound (20.5 mg, 46%). ^{1}H NMR (500 MHz, DMSO-d_6) δ 10.32 (s, 1H), 9.86 (s, 1H), 7.71 (t, J = 9.8, 8.3 Hz, 2H), 7.59 (d, J = 8.3 Hz, 2H), 7.41 (s, 1H), 6.62 (d, J = 2.5 Hz, 1H), 6.51 - 6.41 (m, 2H), 6.28 (dd, J = 17.0, 2.0 Hz, 1H), 5.79 (dd, J = 10.0, 1.9 Hz, 1H), 3.79 (s, 3H), 3.17 (t, J = 4.9 Hz, 4H), 2.45 (t, J = 5.0 Hz, 4H), 2.23 (s, 3H). ^{13}C NMR (126 MHz, DMSO-d_6) δ 181.8, 166.7, 163.8, 141.1, 137.5, 132.2, 128.1, 127.8, 119.1, 107.25, 100.3, 92.9, 56.0, 55.1, 48.5, 46.2. IR $\boldsymbol{\nu}_{max}$ (neat): 2920, 2849, 1672, 1594, 1517, 1409, 968, 762, 727 cm^{-1}. HRMS (ESI) *m/z*: calcd for $C_{25}H_{28}N_6O_3S$ [M + H]$^{+}$, 493.2016; found 493.2016.

3. Expression and purification

A DYRK1A construct comprising the kinase domain (126-490) was cloned into pEXP17 with N-terminal 6x(HIS) affinity tags and TEV protease cleavage sites[17, 18]. Expression was done in shaker flask cultures overnight at 17.8 °C in TB media. For the purification of DYRK1A the cells were resuspended in a lysis buffer containing 50 mM sodium phosphate buffer pH 8.0 with 500 mM NaCl and of 0.5% Tween20. Purification was done via NiNTA columns and an imidazole gradient (10-500 mM), followed by a TEV cleavage overnight and a second NiNTA to separate the kinase from uncut protein and the protease. Final purification for DYRK1A was done via size exclusion chromatography (SEC buffer: 50 mM MOPS pH 6.8, 50 mM KCl, 2 mM β-Me).

4. Crystallization

DYRK1A was concentrated to 7-10 mg/mL in SEC buffer and mixed with inhibitor solutions in DMSO to achieve approximately a 5-10 fold excess of inhibitor. The final concentration of DMSO was ~5%. The protein/inhibitor mixture was than mixed 1:1 with the crystallization solution (100 mM KSCN, 50-100 mM LiCl (or NaCl, or KCl), 10-20% PEG3350) for a final drop size of 4 µl. Crystallization was done in 24 well hanging drop plates. Octahedron shaped crystals appeared within 1-7 days at room temperature. Crystals were cryo-protected with 30% ethylene glycol and flash frozen in liquid nitrogen.

5. Structure solving and refinement

Crystals were measured at the ESRF Grenoble, France. The images were integrated using the software XDSapp[38]. The structure was solved by molecular replacement using the DYRK1A structure 5A4T as a search model. Refinement was done by Phenix[39] and the CCP4[40] program Refmac5[41]. The waters were placed by the program Coot 0.7.2[42]. The crystallographic data and model statistics are summarized in Table S2.

6. Activity assay

The determination of the IC_{50} constants for DYRK1A was done by an ATP regenerative NADH consuming assay[16]. The enzyme velocity was measured at 340 nm over a time period of 300 s at room temperature. ATP and the peptide RRRFRPASPLRGPPK (DYRKtide) were used as substrates. The reaction mixture was composed of 75 µl of 100 mM MOPS buffer pH 6.8, 10 mM KCl, 10 mM MgCl, 1 mM phosphoenolpyruvate, 1 mM DYRKtide, 1 mM β-ME, 15 units/mL lactate dehydrogenase, 10 units/ml pyruvate kinase and 10.7 mM NADH. 10 µl of

~5-20 μM DYRK1A, 2 μL of inhibitor in DMSO in concentrations ranging from 4 nM and 20 μM and 10 μL of ATP 128 μM were added to a total volume of 97 μL. All measurements were done in triplicate at room temperature. All other *in vitro* kinase assays were conducted using the SelectScreen Kinase Profiling Service at Thermo Fisher Scientific (Madison, WI). The protocols are available from Thermo Fisher Scientific website.

7. Cell culture, transfections and treatments

DNA constructs: The plasmid encoding EGFP-tagged DYRK1A has been described earlier[43] and was a kind gift from Dr. D'Arcangelo (Rutgers, USA). The expression vector encoding the FLAG-tagged tau[44] was a kind gift from Dr. Paudel (McGill University, Canada).

NCI-H1299 cells (ATCC-CRL-5803) were maintained in Dulbecco's modified Eagle's medium supplemented with 10% fetal bovine serum (Invitrogen), 2 mM L-glutamine, penicillin (100 U/mL), and streptomycin (100 μg/mL). Lipofectamine LTX (Life Technologies) reagent was used to transfect the cells according to the manufacturer's instructions. The cells were treated for 2 hours with the indicated concentration of compound the day after transfection before they were harvested in MKK-lysis buffer (50 mM Tris/HCl pH 7.5, 1 mM EGTA, 1 mM EDTA, 1% (w/v) Triton-X 100, 1 mM sodium orthovanadate, 50 mM sodium fluoride, 5 mM sodium pyrophosphate and 0.27 M sucrose) and processed for immunoblotting.

8. Immunoblotting

For detection of ectopically expressed FLAG-TAU or EGFP-DYRK1A, the samples were analyzed by SDS-PAGE (4–12% NUPAGE, Life Technologies), transferred to a nitrocellulose membrane (Li-Cor) and probed with a rabbit anti- Phospho-tau-T212 (1:1000) antibody or a mouse monoclonal anti-FLAG antibody. Detection and quantification were performed either

directly using anti-GFP Dylight 800-conjugated antibody or IRDye 800CW-conjugated goat anti-rabbit IgG (H&L) (1:10000) or IRDye 680LT-conjugated donkey anti-mouse IgG (H&L) (1:10000) and the Odyssey Infrared Imaging System (Li-Cor Biosciences). Protein molecular mass was estimated using the MagicMark Western protein standard (Life technologies).

9. Antibodies

The polyclonal antibody against tau phosphorylated at threonine 212 (44-740G) was purchased from (Life Technologies). The monoclonal antibody against FLAG (F1804) was purchased from Sigma-Aldrich. The anti-GFP Dylight 800-conjugated antibody (600-145-215) was purchased from Rockland. The IRDye 800CW-conjugated goat anti-rabbit IgG (H&L) and IRDye 680LT-conjugated donkey anti-mouse IgG (H&L) were purchased from Li-Cor Bioscience.

10. Generation of DYRK1A-NFAT-luc reporter cell line.

The pDEST-LTR-EGFP, a mammalian transfection vector for stable and doxycycline controlled inducible expression of N-terminal-EGFP tagged fusion constructs under the control of a truncated CMV promoter, was a kind gift from Dr. Trond Lamark UiT, Tromsø, Norway[45]. The cDNA encoding human DYRK1A was amplified from the IMAGE clone; IMAGE:100061742 with the following primers:

5-CACCATGCATACAGGAGGAGAGACTTCAGC-3` and

5-TCACGAGCTAGCTACAGGACTCTG-3,

cloned into the pENTR using the pENTR topo cloning kit (Thermo Fischer Scientific). The final pENTR-DYRK1a construct was verified by DNA sequencing. The DYRK1A was transferred from the pENTR-DYRK1A to the vector pDEST-LTR-EGFP to generate the retroviral

expression vector pEXP-LRT-EGFP-DYRK1A using the Gateway LR reaction (Thermo Fischer Scientific).

Phoenix HEK cells were transfected with the pEXP-LRT-EGFP-DYRK1A plasmid using TransIT-LT1 transfection agent (Mirus Bio LLC) following the manufacturer´s protocol. Forty-eight and seventy-two hours later the supernatant were collected and filtered through a 0.45 μm filter. The supernatant was supplemented with 5 μg/mL proteome sulphate and used to transduce the NFAT / LUCPorter™ Stable Reporter HEK Cell Line (Novus Biologicals), which contains express a stable renilla reporter gene under control of a NFAT response element. Two day after the transduction the cell were reseeded in medium containing 5μg/mL blasticidine and blasticidine resistant pools of cells were propagated and tested for expression of EGFP-DYRK1 fusion protein in absence and presence of 1 μg/ml doxycycline. (**Supporting information**)

11. Kinome Profiling.

Kinome profiling was performed using KinomeScan ScanMAX at compound concentration of 10 μM or 1 μM. Data was reported in Supplementary data. Protocols are available from DiscoverX.

ACKNOWLEDGEMENT

We are grateful to Dr. D'Arcangelo ((Rutgers, USA) and Dr. Paudel (McGill, Canada) for providing expression vectors. The work was supported Northern Norway Regional Health Authority/Helse Nord RHF (A.C. and O.M.S.). We acknowledge the European Synchrotron

Radiation Facility for provision of synchrotron radiation facilities. This research was supported by the Research Council of Norway through the grant (247732).

ANCILLARY INFORMATION

Supporting information available: Complete table with all 23 inhibitors, molecular formula strings of the inhibitors, scaffolds of all 23 inhibitors. Crystallographic table of the nine crystal structures, omit maps, surface plots and a superimposition of all the nine inhibitors bound to the ATP pocket of DYRK1A. Table of the kinome scan. Additional tau phosphorylation assays. Overview of the cell based NFAT mediated luciferase reporter gene activity assay including the positive controls. NMR spectra of the compounds.

Accession Codes

PDB codes for DYRK1A complexes: compound **AC12**, 6EIF; compound **AC15**, 6EJ4; compound **AC20**, 6EIJ; compound **AC22**, 6EIL; compound **AC23**, 6EIP; compound **AC24**, 6EIQ; compound **AC25**, 6EIR; compound **AC27**, 6EIS; compound **AC28**, 6EIV.

Authors will release the atomic coordinates and experimental data upon article publication

AUTHOR INFORMATION

Corresponding Author

Corresponding author: *ulli.rothweiler@uit.no

REFERENCES

(1) Qiu, C.; Kivipelto, M.; von Strauss, E. Epidemiology of Alzheimer's disease: occurrence, determinants, and strategies toward intervention. *Dialogues Clin Neurosci* **2009,** *11*, 111-128.

(2) Hardy, J. Alzheimer's disease: the amyloid cascade hypothesis: an update and reappraisal. *J Alzheimers Dis* **2006,** *9*, 151-153.

(3) Hardy, J. A.; Higgins, G. A. Alzheimer's disease: the amyloid cascade hypothesis. *Science* **1992,** *256*, 184-185.

(4) Chetelat, G. Alzheimer disease: A beta-independent processes-rethinking preclinical AD. *Nature Reviews Neurology* **2013,** *9*, 123-124.

(5) Graham, W. V.; Bonito-Oliva, A.; Sakmar, T. P. Update on Alzheimer's disease therapy and prevention strategies. *Annu Rev Med* **2017,** *68*, 413-430.

(6) Lloret, A.; Fuchsberger, T.; Giraldo, E.; Vina, J. Molecular mechanisms linking amyloid beta toxicity and Tau hyperphosphorylation in Alzheimers disease. *Free Radic Biol Med* **2015,** *83*, 186-191.

(7) Ferrer, I.; Barrachina, M.; Puig, B.; de Lagran, M. M.; Marti, E.; Avila, J.; Dierssen, M. Constitutive Dyrk1A is abnormally expressed in Alzheimer disease, Down syndrome, Pick disease, and related transgenic models. *Neurobiology of Disease* **2005,** *20*, 392-400.

(8) Dierssen, M. Down syndrome: the brain in trisomic mode. *Nature Reviews Neuroscience* **2012,** *13*, 844-858.

(9) Ryoo, S. R.; Cho, H. J.; Lee, H. W.; Jeong, H. K.; Radnaabazar, C.; Kim, Y. S.; Kim, M. J.; Son, M. Y.; Seo, H.; Chung, S. H.; Song, W. J. Dual-specificity tyrosine(Y)-phosphorylation regulated kinase 1A-mediated phosphorylation of amyloid precursor protein: evidence for a

functional link between Down syndrome and Alzheimer's disease. *Journal of Neurochemistry* **2008,** *104*, 1333-1344.

(10) Ryu, Y. S.; Park, S. Y.; Jung, M. S.; Yoon, S. H.; Kwen, M. Y.; Lee, S. Y.; Choi, S. H.; Radnaabazar, C.; Kim, M. K.; Kim, H.; Kim, K.; Song, W. J.; Chung, S. H. Dyrk1A-mediated phosphorylation of Presenilin 1: a functional link between Down syndrome and Alzheimer's disease. *Journal of Neurochemistry* **2010,** *115*, 574-584.

(11) Liu, F.; Liang, Z. H.; Wegiel, J.; Hwang, Y. W.; Iqbal, K.; Grundke-Iqbal, I.; Ramakrishna, N.; Gong, C. X. Overexpression of Dyrk1A contributes to neurofibrillary degeneration in Down syndrome. *Faseb Journal* **2008,** *22*, 3224-3233.

(12) Wegiel, J.; Gong, C. X.; Hwang, Y. W. The role of DYRK1A in neurodegenerative diseases. *Febs Journal* **2011,** *278*, 236-245.

(13) Belgardt, B. F.; Lammert, E. DYRK1A: A promising drug target for islet transplant-based diabetes therapies. *Diabetes* **2016,** *65*, 1496-1498.

(14) Dirice, E.; Walpita, D.; Vetere, A.; Meier, B. C.; Kahraman, S.; Hu, J.; Dancik, V.; Burns, S. M.; Gilbert, T. J.; Olson, D. E.; Clemons, P. A.; Kulkarni, R. N.; Wagner, B. K. Inhibition of DYRK1A stimulates human beta-cell proliferation. *Diabetes* **2016,** *65*, 1660-1671.

(15) Wang, P.; Alvarez-Perez, J. C.; Felsenfeld, D. P.; Liu, H. T.; Sivendran, S.; Bender, A.; Kumar, A.; Sanchez, R.; Scott, D. K.; Garcia-Ocana, A.; Stewart, A. F. A high-throughput chemical screen reveals that harmine-mediated inhibition of DYRK1A increases human pancreatic beta cell replication. *Nature Medicine* **2015,** *21*, 383-388.

(16) Cook, P. F.; Neville, M. E., Jr.; Vrana, K. E.; Hartl, F. T.; Roskoski, R., Jr. Adenosine cyclic 3',5'-monophosphate dependent protein kinase: kinetic mechanism for the bovine skeletal muscle catalytic subunit. *Biochemistry* **1982,** *21*, 5794-5799.

(17) Alexeeva, M.; Aberg, E.; Engh, R. A.; Rothweiler, U. The structure of a dual-specificity tyrosine phosphorylation-regulated kinase 1A-PKC412 complex reveals disulfide-bridge formation with the anomalous catalytic loop HRD(HCD) cysteine. *Acta Crystallogr D Biol Crystallogr* **2015,** *71*, 1207-1215.

(18) Rothweiler, U.; Stensen, W.; Brandsdal, B. O.; Isaksson, J.; Leeson, F. A.; Engh, R. A.; Svendsen, J. S. Probing the ATP-binding pocket of protein kinase DYRK1A with benzothiazole fragment molecules. *J Med Chem* **2016,** *59*, 9814–9824.

(19) Tahtouh, T.; Elkins, J. M.; Filippakopoulos, P.; Soundararajan, M.; Burgy, G.; Durieu, E.; Cochet, C.; Schmid, R. S.; Lo, D. C.; Dehommel, F.; Oberhozer, A. E.; Pearl, L. H.; Carreaux, F.; Bazureau, J. P.; Knapp, S.; Meijer, L. Selectivity, cocrystal structures, and neuroprotective properties of leucettines, a family of protein kinase inhibitors derived from the marine sponge alkaloid leucettamine B. *J Med Chem* **2012,** *55*, 9312-9330.

(20) Choi, H. G.; Zhang, J. M.; Weisberg, E.; Griffin, J. D.; Sim, T.; Gray, N. S. Development of 'DFG-out' inhibitors of gatekeeper mutant kinases. *Bioorg Med Chem Lett* **2012,** *22*, 5297-5302.

(21) Liu, Q. S.; Wang, J. H.; Kang, S. A.; Thoreen, C. C.; Hur, W.; Ahmed, T.; Sabatini, D. M.; Gray, N. S. Discovery of 9-(6-aminopyridin-3-yl)-1-(3-(trifluoromethyl)-phenyl)benzo[h][1,6]naphthyridin-2(1H)-one (Torin2) as a potent, selective, and orally available mammalian target of raparnycin (mTOR) inhibitor for treatment of cancer. *J Med Chem* **2011,** *54*, 1473-1480.

(22) Nguyen, T. L.; Fruit, C.; Herault, Y.; Meijer, L.; Besson, T. Dual-specificity tyrosine phosphorylation-regulated kinase 1A (DYRK1A) inhibitors: a survey of recent patent literature. *Expert Opin Ther Pat* **2017,** *11*, 1-17.

(23) Ogawa, Y.; Nonaka, Y.; Goto, T.; Ohnishi, E.; Hiramatsu, T.; Kii, I.; Yoshida, M.; Ikura, T.; Onogi, H.; Shibuya, H.; Hosoya, T.; Ito, N.; Hagiwara, M. Development of a novel selective inhibitor of the Down syndrome-related kinase Dyrk1A. *Nat Commun* **2010,** *1*, 86.

(24) Masaki, S.; Kii, I.; Sumida, Y.; Kato-Sumida, T.; Ogawa, Y.; Ito, N.; Nakamura, M.; Sonamoto, R.; Kataoka, N.; Hosoya, T.; Hagiwara, M. Design and synthesis of a potent inhibitor of class 1 DYRK kinases as a suppressor of adipogenesis. *Bioorgan Med Chem* **2015,** *23*, 4434-4441.

(25) Ruben, K.; Wurzlbauer, A.; Walte, A.; Sippl, W.; Bracher, F.; Becker, W. Selectivity profiling and biological activity of novel beta-carbolines as potent and selective DYRK1 kinase inhibitors. *PLoS One* **2015,** *10*.

(26) De la Torre, R.; De Sola, S.; Pons, M.; Duchon, A.; de Lagran, M. M.; Farre, M.; Fito, M.; Benejam, B.; Langohr, K.; Rodriguez, J.; Pujadas, M.; Bizot, J. C.; Cuenca, A.; Janel, N.; Catuara, S.; Covas, M. I.; Blehaut, H.; Herault, Y.; Delabar, J. M.; Dierssen, M. Epigallocatechin-3-gallate, a DYRK1A inhibitor, rescues cognitive deficits in Down syndrome mouse models and in humans. *Mol Nutr Food Res* **2014,** *58*, 278-288.

(27) Coutadeur, S.; Benyamine, H.; Delalonde, L.; de Oliveira, C.; Leblond, B.; Foucourt, A.; Besson, T.; Casagrande, A. S.; Taverne, T.; Girard, A.; Pando, M. P.; Desire, L. A novel DYRK1A (dual specificity tyrosine phosphorylation-regulated kinase 1A) inhibitor for the treatment of Alzheimer's disease: effect on Tau and amyloid pathologies in vitro. *J Neurochem* **2015,** *133*, 440-451.

(28) Chaikuad, A.; Diharce, J.; Schroder, M.; Foucourt, A.; Leblond, B.; Casagrande, A. S.; Desire, L.; Bonnet, P.; Knapp, S.; Besson, T. An unusual binding model of the methyl 9-anilinothiazolo[5,4-f] quinazoline-2-carbimidates (EHT 1610 and EHT 5372) confers high

selectivity for dual-specificity tyrosine phosphorylation-regulated kinases. *J Med Chem* **2016,** *59*, 10315-10321.

(29) Naert, G.; Ferre, V.; Meunier, J.; Keller, E.; Malmstrom, S.; Givalois, L.; Carreaux, F.; Bazureau, J. P.; Maurice, T. Leucettine L41, a DYRK1A-preferential DYRKs/CLKs inhibitor, prevents memory impairments and neurotoxicity induced by oligomeric A beta(25-35) peptide administration in mice. *Eur Neuropsychopharm* **2015,** *25*, 2170-2182.

(30) Rothweiler, U.; Eriksson, J.; Stensen, W.; Leeson, F.; Engh, R. A.; Svendsen, J. S. Luciferin and derivatives as a DYRK selective scaffold for the design of protein kinase inhibitors. *Eur J Med Chem* **2015,** *94*, 140-148.

(31) Kii, I.; Sumida, Y.; Goto, T.; Sonamoto, R.; Okuno, Y.; Yoshida, S.; Kato-Sumida, T.; Koike, Y.; Abe, M.; Nonaka, Y.; Ikura, T.; Ito, N.; Shibuya, H.; Hosoya, T.; Hagiwara, M. Selective inhibition of the kinase DYRK1A by targeting its folding process. *Nat Commun* **2016,** *7*, 11391.

(32) Hong, S.; Kim, J.; Seo, J. H.; Jung, K. H.; Hong, S. S.; Hong, S. Design, synthesis, and evaluation of 3,5-disubstituted 7-azaindoles as Trk inhibitors with anticancer and antiangiogenic activities. *J Med Chem* **2012,** *55*, 5337-5349.

(33) Choi, H. G., Sim, T., Gray, N., Zhou, W., Chang, J. W, Zhang, J., Weisberg, E. Fused Heterocyclic Compounds and their Uses, PCT Int. Appl., WO 2010144909 A1 20101216. 2010.

(34) Miduturu, C. V.; Deng, X.; Kwiatkowski, N.; Yang, W.; Brault, L.; Filippakopoulos, P.; Chung, E.; Yang, Q.; Schwaller, J.; Knapp, S.; King, R. W.; Lee, J. D.; Herrgard, S.; Zarrinkar, P.; Gray, N. S. High-throughput kinase profiling: a more efficient approach toward the discovery of new kinase inhibitors. *Chem Biol* **2011,** *18*, 868-879.

(35) Liu, Q.; Wang, J.; Kang, S. A.; Thoreen, C. C.; Hur, W.; Ahmed, T.; Sabatini, D. M.; Gray, N. S. Discovery of 9-(6-aminopyridin-3-yl)-1-(3-

(trifluoromethyl)phenyl)benzo[h][1,6]naphthyridin-2(1H)-one (Torin2) as a potent, selective, and orally available mammalian target of rapamycin (mTOR) inhibitor for treatment of cancer. *J Med Chem* **2011,** *54*, 1473-1480.

(36) Lee, S.; Shang, Y.; Redmond, S. A.; Urisman, A.; Tang, A. A.; Li, K. H.; Burlingame, A. L.; Pak, R. A.; Jovicic, A.; Gitler, A. D.; Wang, J.; Gray, N. S.; Seeley, W. W.; Siddique, T.; Bigio, E. H.; Lee, V. M.; Trojanowski, J. Q.; Chan, J. R.; Huang, E. J. Activation of HIPK2 promotes ER stress-mediated neurodegeneration in amyotrophic lateral sclerosis. *Neuron* **2016,** *91*, 41-55.

(37) Bruce, I., Budd, E., Edwards, L., Howsham, C. Pyridines and Pyrazines as Inhibitors of Pi3k, PCT Int. Appl., WO 2009115517 A2 20090924. 2009.

(38) Krug, M.; Weiss, M. S.; Heinemann, U.; Mueller, U. XDSAPP: a graphical user interface for the convenient processing of diffraction data using XDS. *J Appl Crystallogr* **2012,** *45*, 568-572.

(39) Adams, P. D.; Afonine, P. V.; Bunkoczi, G.; Chen, V. B.; Davis, I. W.; Echols, N.; Headd, J. J.; Hung, L. W.; Kapral, G. J.; Grosse-Kunstleve, R. W.; McCoy, A. J.; Moriarty, N. W.; Oeffner, R.; Read, R. J.; Richardson, D. C.; Richardson, J. S.; Terwilliger, T. C.; Zwart, P. H. PHENIX: a comprehensive Python-based system for macromolecular structure solution. *Acta Crystallogr D Biol Crystallogr* **2010,** *66*, 213-221.

(40) Winn, M. D.; Ballard, C. C.; Cowtan, K. D.; Dodson, E. J.; Emsley, P.; Evans, P. R.; Keegan, R. M.; Krissinel, E. B.; Leslie, A. G.; McCoy, A.; McNicholas, S. J.; Murshudov, G. N.; Pannu, N. S.; Potterton, E. A.; Powell, H. R.; Read, R. J.; Vagin, A.; Wilson, K. S. Overview of the CCP4 suite and current developments. *Acta Crystallogr D Biol Crystallogr* **2011,** *67*, 235-242.

(41) Murshudov, G. N.; Skubak, P.; Lebedev, A. A.; Pannu, N. S.; Steiner, R. A.; Nicholls, R. A.; Winn, M. D.; Long, F.; Vagin, A. A. REFMAC5 for the refinement of macromolecular crystal structures. *Acta Crystallogr D Biol Crystallogr* **2011,** *67*, 355-367.

(42) Emsley, P.; Lohkamp, B.; Scott, W. G.; Cowtan, K. Features and development of Coot. *Acta Crystallogr D Biol Crystallogr* **2010,** *66*, 486-501.

(43) Yabut, O.; Domogauer, J.; D'Arcangelo, G. Dyrk1A overexpression inhibits proliferation and induces premature neuronal differentiation of neural progenitor cells. *Journal of Neuroscience* **2010,** *30*, 4004-4014.

(44) Li, T.; Paudel, H. K. Glycogen synthase kinase 3 beta phosphorylates Alzheimer's disease-specific Ser(396) of microtubule-associated protein tau by a sequential mechanism. *Biochemistry* **2006,** *45*, 3125-3133.

(45) Skytte Rasmussen, M.; Mouilleron, S.; Kumar Shrestha, B.; Wirth, M.; Lee, R.; Bowitz Larsen, K.; Abudu Princely, Y.; O'Reilly, N.; Sjottem, E.; Tooze, S. A.; Lamark, T.; Johansen, T. ATG4B contains a C-terminal LIR motif important for binding and efficient cleavage of mammalian orthologs of yeast Atg8. *Autophagy* **2017,** *13*, 834-853.

Table of Contents graphic